Journal of Non-Crystalline Solids 610 (2023) 122311

Contents lists available at ScienceDirect

Journal of Non-Crystalline Solids

journal homepage: www.elsevier.com/locate/jnoncrysol

Thermophysical parameters governing the glass formation and crystallization of CuZr

Alberto Castellero *, Livio Battezzati

Dipartimento di Chimica, Università di Torino, Via Pietro Giuria 7, Torino 10125, Italy

ARTICLE INFO

Keywords:
Metallic glass
Thermophysical properties
Classical nucleation theory
Crystallization
TTT curve
CCT curve

ABSTRACT

Cu-Zr is one of the best binary metallic glass formers. Here, new data on the enthalpy and specific heat difference between undercooled melt and crystal phases are provided for the equiatomic composition CuZr. Together with a comprehensive collection of literature data on the heat of crystallization and fusion, on the viscosity and crystal growth rate, the parameters needed for the application of the Classical Nucleation Theory are assessed. The TTT and CCT curves for crystallization are computed allowing the determination of the crystal-liquid interfacial energy by fitting the critical cooling rate for bulk glass formation.

The glass forming tendency of CuZr is discussed pointing to the role of the high interfacial energy and the sluggish interdiffusion in the undercooled melt.

1. Introduction

The Cu-Zr system is a binary glass-former where amorphization occurs in a large composition range including stoichiometric intermetallics and bulk glass formation was demonstrated. Starting from early studies of rapid solidification, it has been taken as paradigmatic for studying the glass-forming ability of metallic alloys (i.e. the avoidance of crystal nucleation from the liquid) [1–5].

A comprehensive recent study employing electrostatically levitated samples has provided a set of data for quantities (heat of fusion, viscosity, specific volume) appearing in the classical nucleation theory [6, 7]. The time for nucleation at various temperatures and the undercoolability on free cooling after laser melting was experimentally determined. This allowed to derive the activation barrier for nucleation, ΔG^*

$$\Delta G^* = \frac{16\pi}{3}\frac{\sigma^3}{(\Delta G_v)^2} f(\theta) \tag{1}$$

where ΔG_v is the free energy difference between liquid and crystal phases, σ is the liquid-crystal interfacial energy and $f(\theta)$ is a function of the wetting angle θ for the heterogeneous nucleation that becomes equal to 1 for the homogeneous case. According to the Classical Nucleation Theory (CNT), the nucleation frequency is given by

$$I_v = \frac{24Dn^*}{\lambda^2} Z N_A exp\left(\frac{-\Delta G^*}{RT}\right) \tag{2}$$

where D is the diffusion coefficient, n^* is the number of atoms in the nucleus of critical size, λ is the jump distance, Z is the Zeldovich factor, N_A is the Avogadro number, R is the gas constant.

Using the Thompson-Spaepen approximation for the free energy difference between the melt undercooled at temperature, T, and equilibrium crystal phase, [8],

$$\Delta G_v = \frac{\Delta H_f (T_f - T)}{T_f}\frac{2}{T_f + T} \tag{3}$$

where, ΔH_f is the heat of fusion and T_f, the melting point, the liquid-crystal interfacial energy was determined as the only parameter remaining unknown [7]. The values appear very plausible in the range 0.12–0.14 $J{\cdot}m^{-2}$ for various alloy compositions. It is worth mentioning that the undercoolability correlated reasonably with the critical casting thickness of bulk glasses [6].

In recent contributions on levitated samples processed on board of the International Space Station the viscosity data were confirmed [9] and a set of data on the specific heat, C_p, of liquid equiatomic CuZr were provided as a function of temperature [10].

This paper reports laboratory data on the heat of crystallization and the difference in specific heat between undecooled liquid and crystal phase, ΔC_p, with which the whole set of thermophysical properties of

* Corresponding author.
E-mail address: alberto.castellero@unito.it (A. Castellero).

https://doi.org/10.1016/j.jnoncrysol.2023.122311
Received 15 February 2023; Received in revised form 17 March 2023; Accepted 27 March 2023
Available online 30 March 2023

undercooled equiatomic CuZr is revised allowing the calculation of ΔG_v from experimental data and the verification of the estimate of σ.

The experimental data are supported by the results of a detailed literature overview of measurements available on quantities needed to apply the CNT, allowing the calculation of the time-temperature-transformation (TTT) and continuous cooling transformation (CCT) curves for CuZr to be confronted with the experimental critical cooling rate (CCR) for glass formation.

2. Experimental

The CuZr master alloy was prepared by melting the elemental metals under Ar atmosphere in an arc furnace (Edmund Bühler GmbH). Amorphous ribbons were obtained using a planar flow casting apparatus (Edmund Bühler GmbH). Structural characterization of the samples was performed by X-ray diffraction (Panalytical X'Pert Pro) using Bragg-Brentano geometry and Cu kα radiation.

Differential scanning calorimetry (DSC) was employed to measure the ΔC_p in the temperature region of the glass transition, the temperature and the heat of crystallization of the amorphous ribbons as a function of heating rate (Pyris Diamond DSC Perkin Elmer) employing 2, 20, 40, 100, 200 K·min^{-1}. The DSC equipment was calibrated using both sapphire and metallic standards. High temperature DSC measurements (Setaram HT-DSC) allowed to evaluate the heat of fusion and the heat of solidification of the alloy upon heating and cooling (10 K·min^{-1}), respectively.

3. Results and discussion

3.1. Heat of fusion/solidification

The data on the heat of fusion, ΔH_f, in the literature are controversial. Specifically, the value given in Ref. [11] (9219 J·mol^{-1}) was employed later by the same group and other authors in discussing results on the growth rate of crystals from the CuZr undercooled melt [12–15]. The value given by Ganorkar et al. [6] is substantially higher (11,200 J·mol^{-1}). Therefore, new measurements were made by HTDSC for this work giving the heat of fusion at 1208 K and solidification in slightly undercooling regime at 1163 K as 9100 ± 100 J·mol^{-1} confirming the results in Ref. [11]. *In situ* X ray diffraction experiments, run using synchrotron radiation, showed that the solidification product is the B2 CuZr phase [16].

3.2. Heat of crystallization

Fig. 1 with inset shows representative DSC traces of an amorphous ribbon of CuZr.

Data on the heat of crystallization, ΔH_x, of melt spun metallic glasses, as a function of heating rate are given in Fig. 2. The ΔH_x increases as a function of the increase in crystallization temperature due to the increase in heating rate. The figure reports also values of ΔH_x on CuZr appeared over the years in the literature [1,3,17–19] and the value obtained by fast calorimetry at the heating rate of 4000 K·s^{-1} on sputter deposited thin films whose crystallization occurs at intermediate temperature between the glass transition on the melting point of the alloy [20]. As a confirmation of the above reports.

The overall trend of the enthalpy difference between undercooled/stable liquid and crystal phase from the melting point and below is consistent among all the data obtained with the respective alloys in different laboratories within the scatter of about 0.5 kJ·mol^{-1} which is justified by technical aspects of the measurements (e.g. equipment calibration, baseline construction) and by the occurrence of minor heat effects due to crystallization of metastable compounds which was already recognized in Ref. [17] affecting the measurement. The curves in the figure were calculated according to

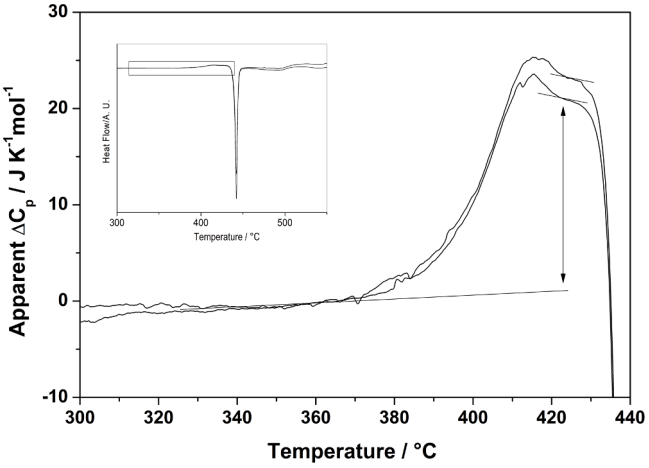

Fig. 1. Representative DSC traces (20 K/min) of an amorphous ribbon of CuZr for the determination of the apparent specific heat difference between the undercooled liquid and the glass. Here the specific heat of the glass just below the glass transition is taken as reference state. A single average value of the specific heat difference in the undercooling regime was taken for every heating run.

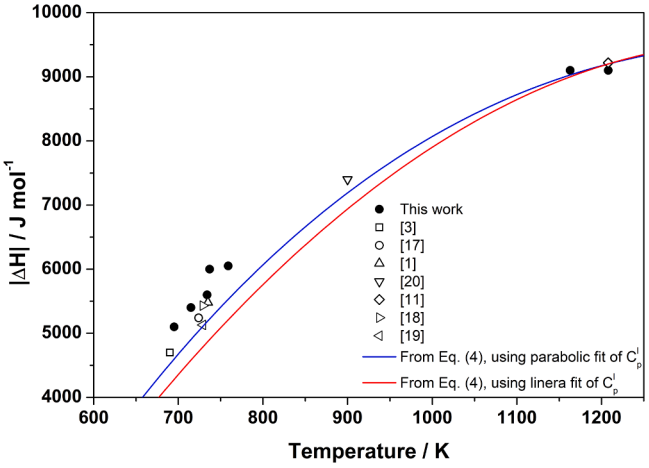

Fig. 2. Absolute value of the enthalpy difference between undercooled liquid (or glass) and crystal phases of CuZr as a function of temperature. Full symbols: present work; △ [1]; □ [3]; ◇ [11]; ○ [17]; ▷ [18]; ◁ [19]; ▽ [20].

$$\Delta H_x = \Delta H_f - \int_T^{T_f} \Delta C_p dT \tag{4}$$

where ΔH_f, T_f and ΔC_p are the enthalpy of fusion, the melting temperature and the difference between the specific heat of the liquid (C_p^l) and the solid (C_p^s), respectively. The two curves show the enthalpy difference calculated by using the assessed heat of fusion and the specific heat difference discussed in the next paragraph.

3.3. Liquid specific heat

Fig. 3 reports the specific heat of CuZr in the liquid phase as given in Ref. [10] and the values computed in this work by summing the experimental difference in specific heat in the deep undercooling regime between undercooled liquid and crystal phase, ΔC_p, (Fig. 1) and the specific heat of the crystal phase computed according to the additive Neumann-Kopp rule employing assessed data of Ref. [21].

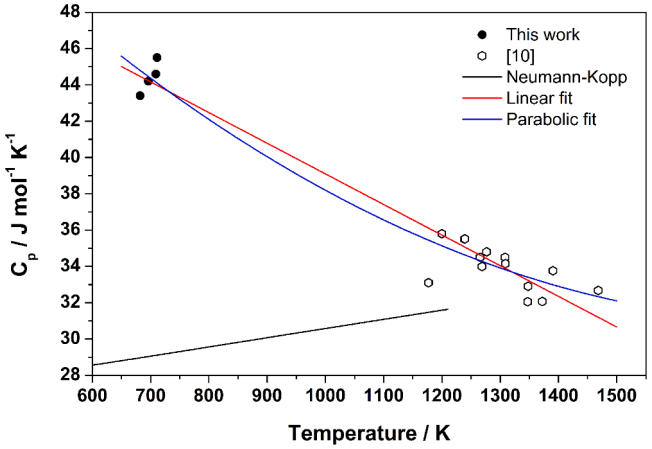

Fig. 3. Specific heat of CuZr as a function of temperature. Symbols give experimental values of the specific heat difference between undercooled liquid and solid phases (filled circles, this work) and of the specific heat of the liquid (open symbols [10]). The blue and red lines represents the parabolic and linear fits of the experimental data for the liquid. The black line gives the specific heat of the crystalline CuZr solid phase, calculated according to the Neumann-Kopp rule.

The resulting specific heat of the liquid phase with either a linear and parabolic fit is

$$C_p^l = 55.979 - 0.01688 \cdot T \Big/ \text{Jmol}^{-1} \quad \text{linear fit} \tag{5}$$

$$C_p^l = 66.053 - 0.03829 \cdot T + 1.0436 \cdot 10^{-5} \cdot T^2 \Big/ \text{J mol}^{-1} \quad \text{parabolic fit} \tag{6}$$

3.4. Free energy difference between undercooled melt and equilibrium crystal phase

The molar free energy difference between liquid and equilibrium crystal phases is computed according to

$$\Delta G = \Delta H_f - \int_T^{T_f} \Delta C_p dT - T\Delta S_f + T \int_T^{T_f} \Delta C_p \frac{dT}{T} \tag{7}$$

where all the quantities were defined in Section 3.2, except ΔS_f that represents the entropy of fusion.

The difference in molar free energy between undercooled liquid and crystal phase, ΔG, is reported in Fig. 4 using either linear and parabolic fits of C_p^l, together with that computed with the Thompson-Spaepen formula. The deviation of the latter curve with respect to the two curves derived from experimental data is up to 15% in the glass transition region.

3.5. Liquid viscosity

All available viscosity data [7,9,22–25] for the equilibrium and undercooled CuZr liquid are collected in Fig. 5. At lower temperature, the viscosity near the glass transition region is taken from the only available contribution in Ref. [22], that was obtained by dynamic mechanical analysis. At higher temperature, data from Ref. [9] were measured on board the International Space Station while all the others were determined on ground. In the latter case, there is a good agreement among the different sets of data. Some deviation from the overall trend is seen at the highest undercooling (below 1100 K) for those by Lagogianni et al. [25] which, however, were obtained with the same oscillation drop technique as the others.

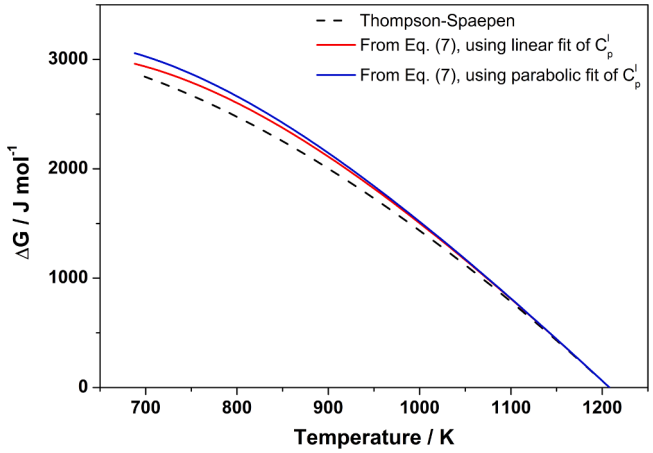

Fig. 4. Temperature dependence of the Gibbs free energy difference between undercooled liquid and crystalline phase computed with Eq. (7), using the linear (red continuous line) and parabolic (blues continuous line) fits of C_p^l from Fig. 3, and with the Thompson-Spaepen model (dashed black line).

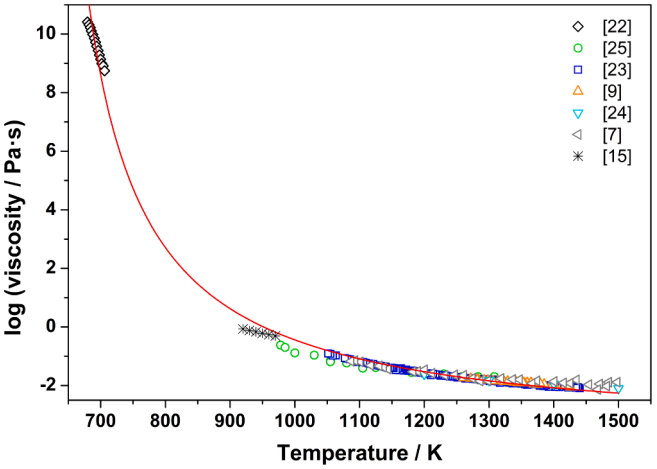

Fig. 5. Temperature dependence of the viscosity of the CuZr liquid. Open symbols give values as measured in Refs. [7,9,22–25], that were fitted all together with the VFT equation (red continuous line). Stars represent the viscosity calculated using the Stokes-Einstein equation and values of the diffusivity coefficient estimated from growth rate measurements [15].

The overall set of data was fitted with the Vogel-Fulker-Tammann (VFT) equation

$$\eta = \eta_0 \exp\left(\frac{B}{T - T_0}\right) \tag{8}$$

obtaining $\eta_0 = 1.78 \cdot 10^{-4}$ Pa·s, $B = 3118$ K, $T_0 = 590$ K. In comparison, when fitting only data from Ref. [7] and Ref. [22], Ganorkar et al. [7] obtained rather close parameters, i.e. $\eta_0 = 2.3 \cdot 10^{-4}$ Pa·s, $B = 2874$ K, $T_0 = 603$ K. The general agreement of experiments on the viscosity provides a sound basis for discussing the mobility in liquid CuZr.

Data on growth rate (u_c) of CuZr crystals are available in the same temperature range of the measurements of liquid viscosity [15]. It was shown that growth is diffusion controlled, allowing the estimation of the temperature dependence of the interdiffusion coefficient (D) through the following relationships

$$u_c = \frac{f}{\lambda} D \left[1 - exp\left(\frac{-\Delta G}{RT}\right)\right] \tag{9}$$

$$D = D_0 exp\left(-\frac{Q}{RT}\right) \tag{10}$$

where f is a geometrical factor ($\sim$ 1), λ is the interatomic spacing ($\sim$ 2 Å), D_0 is the pre-exponential factor for diffusivity and Q is the activation energy for diffusion.

Using the Stokes-Einstein equation linking diffusivity (D) to viscosity (η)

$$D = \frac{k_B T}{6\pi r \eta} \tag{11}$$

where k_B is the Boltzmann constant and r is the ionic radius, the viscosity was estimated, as reported in Fig. 5 with filled symbols. The values obtained fall within less than an order of magnitude of the experimental values for viscosity.

3.6. TTT and CCT curves

Using Eq. (2), the nucleation frequency for the homogeneous case was determined as a function of temperature. D was estimated through the Stokes-Einstein relationship using the VFT fit that gives the temperature dependence of viscosity, n^* is computed from the size of the critical nucleus and the average atomic volume in the alloy, Z is assumed of the order of 10^{-1} for the present case, in ΔG^* the ΔG_v is obtained from the experimental data previously discussed, while the interfacial energy is set as a free parameter.

The time for reaching a given transformed fraction at each temperature, $x(T)$, is obtained from

$$x(T) = 1 - exp\left(-\frac{\pi}{3} I_v u_c^n t^{n+1}\right) \tag{12}$$

assuming an Avrami exponent n equal to 3 (i.e. three-dimensional growth), taken as the average of the values reported in Ref. [26] and Ref. [27], and a transformed fraction of 10^{-6}.

The same transformed fraction is also obtained on continuous cooling at a rate q at temperatures satisfying the following equation [28]

$$x(T) = \left[\frac{1}{q}\int_{T_m}^{T} \frac{dT}{t_{100}(T)}\right]^4 \tag{13}$$

where $t_{100}(T)$ is the time needed to complete the transformation at each temperature.

The TTT and CCT curves for the crystallization of CuZr from the undercooled liquid computed according to Eq. (12) and Eq. (13), respectively, are reported in Fig. 6. All thermophysical properties, except the interfacial energy, are now available from experimental data. The CCT curve is calculated assuming the value of 0.1336 J·m^{-2} for the interfacial energy in order to match the calculated critical cooling rate for crystallization with the experimental value ($\sim$250 K·s^{-1}) estimated by Wang et al. [29]. Once the value of the interfacial energy is fixed, the calculated TTT curve satisfactorily fits the experimental data (empty triangles in Fig. 6) for the isothermal crystallization obtained by Ganorkar et al. [6,7]. The value of interfacial energy lays on the upper limit suggested in Ref. [7].

The available data for the beginning of the crystallization of CuZr glasses (half-filled symbols in Fig. 6), obtained by isothermal DSC measurements in various reports [26,27,30,31], are not fitted by the TTT curve calculated assuming homogeneous nucleation (continuous red line in Fig. 6) since the latter is located at much longer times with respect to the experimental data. This suggests that the nucleation taking place in the crystallization studies is heterogeneous. Assuming ZrO_2 as the nucleating agent, due to the high affinity of Zr for oxygen, the wetting angle between the liquid and the crystal phase to be employed in the spherical cap model [32] can be approximated to 60°, as found in Ref. [33] by means of wetting experiments. The resulting TTT curve

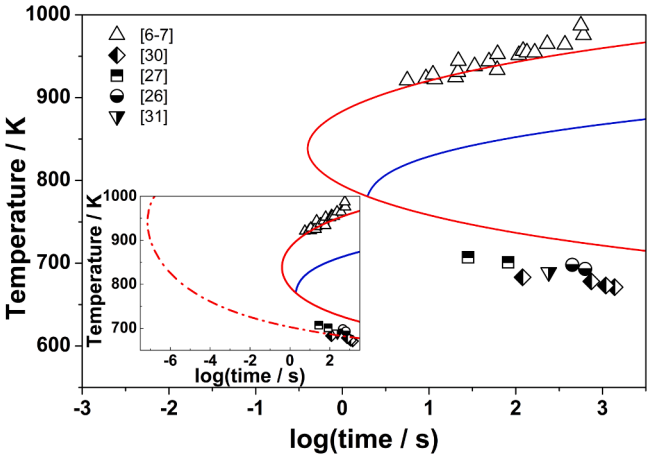

Fig. 6. Computed TTT (red lines) and CCT (blue line) curves for the beginning of the crystallization of CuZr (transformed fraction of 1 part per million). Continuous and dash-dot lines refer to homogeneous and heterogeneous nucleation, respectively. Empty triangles give experimental data for the isothermal crystallization of the undercooled liquid [6,7], half-filled symbols give experimental data for the isothermal crystallization of amorphous CuZr [26,27,30,31].

(dash-dot red line) falls at lower times of orders of magnitude with respect to the previous one allowing to fit the experimental data of the isothermal crystallization (inset of Fig. 6). However, when heterogeneous nucleation is considered, the corresponding TTT curve (dash-dot red line) strongly underestimate the time required for the beginning of the isothermal crystallization from the liquid at higher temperature [6,7]. These findings suggest that different mechanisms for nucleation (i.e., homogeneous and heterogeneous) should be considered for the crystallization of CuZr from the liquid and the glass in the respective temperature ranges.

3.7. Glass forming tendency

The free energy difference between liquid and CuZr follows the downwards bending typical of metallic glass-formers on undercooling [8]. Similarly typical is the overall trend of viscosity with value at the melting point of 0.025 Pa·s in line with that of deep eutectic melts [34], and the fragility index at the glass transition of the order of 50 [22].

The Glass Forming Tendency is apparently related the low melting point of Cu-Zr intermetallics in the center of the phase diagram. This follows the trend of CCR computed for $Cu_{100-x}Zr_x$ (x = 1–10) by molecular dynamics simulation [35] where the increase in Zr content caused a change of the value of CCR of orders of magnitude although still much higher than that of equiatomic CuZr. The assessment of thermodynamic properties showed the limited thermodynamic stability of intermetallic phases with respect to the liquid in the composition range at the center of the phase diagram [36]. They also display sluggish nucleation tendency. Actually, the stronger competitor for glass formation was indicated as the $Cu_{51}Zr_{14}$ compound, i.e. the one having the highest melting point although a different composition with respect to equiatomic CuZr [29]. It should also be mentioned that another high–melting compound, Cu_8Zr_3, was found to compete with glass formation in the respective composition range [5].

Resorting to the homogeneous nucleation theory in computing the TTT and CCT curves is justified by the agreement with quenching and crystallization experiments in containerless processing. A possible role of impurity oxygen cannot be ruled out. However, the CCR of alloys containing various amounts of oxygen resulted of the order of 10^3 –10^2 K·s^{-1} [4]. We modified the interfacial energy to match these CCR. The differences fall in a range of 0.002 J·m^{-2}, not enough to discriminate between different oxygen contents.

Overall, the solid-liquid interfacial energy derived from the fitting of experimental data (0.1336 $J{\cdot}m^{-2}$) appears as a decisive parameter in explaining the sluggish nucleation kinetics in CuZr. In fact, small variation of the interfacial energy strongly affects the CCR value (e.g. ~ 140 K/s and ~ 600 K/s when σ is 0.134 $J{\cdot}m^{-2}$ and 0.133 $J{\cdot}m^{-2}$, respectively). The value of 0.1336 $J{\cdot}m^{-2}$ is high in comparison with the average crystal-liquid interfacial energy for metals which is given by $0.55{\cdot}\Delta H_f$ on a molar basis [37], resulting 0.1236 $J{\cdot}m^{-2}$ with the use of the molar volume of $1.05{\cdot}10^{-5}$ $m^3{\cdot}mol^{-1}$ [11]. Should this value be used in the equation for nucleation, the TTT and CCT curves would be shifted to much shorter times far away from the experimental data.

The other parameter helping in the explanation of the good glass forming tendency of CuZr is the diffusion coefficient which must be derived from viscosity by using the Stokes-Einstein equation. The diffusivity of the fast element Cu, in fact, is about four orders of magnitude higher than the *D* computed from viscosity in the temperature range above the glass transition [38]. Should the diffusion of Cu be the rate determining step for atomic attachment to the nucleus, again a pronounced shift in the times for TTT and CCT curves would occur. This supports the decoupling of Cu diffusion from viscous flow found in Ref. [38].

On the other hand, the isothermal crystallization of CuZr glasses in the undercooling regime just above the glass transition region takes much less time than predicted by the TTT curve [26,27,30,31]. In order to match these times heterogeneous nucleation must be considered.

4. Conclusions

This work provides new data of the heat of crystallization, the heat of fusion, and the difference in specific heat between undercooled liquid and glass in the region of the glass transition of equiatomic CuZr. Together with a critical collection of literature data on thermodynamic and transport properties of undercooled CuZr a full set of thermophysical parameters needed for the application of the CNT is obtained leaving the crystal-liquid interfacial energy, σ, as the only free parameter.

The CCT curve is computed by adjusting the value of σ in order to match the critical cooling rate for bulk glass formation available in the literature. With this the TTT curve fits well the experimental isothermal times for crystallization in the undercooling regime reported in Refs. [6,7]. The value of the interfacial energy obtained here, 0.1336 $J{\cdot}m^{-2}$, is slightly lower than the upper limit derived in Ref. [7] (0.14 $J{\cdot}m^{-2}$), although the difference is significant due to the sensitivity of the position of the TTT curve on the time scale to this parameter.

This value is about 20% higher with respect to the value expected if the average interfacial energy of metals at the melting point was considered. This appears a substantial factor explaining the good glass forming tendency of binary CuZr together with the depression of the melting point of the compound stemming from its limited thermodynamic stability in comparison with the corresponding liquid phase.

The sluggish nucleation of CuZr from the undercooled melt is also favoured by the sluggish atomic interdiffusion which appears to be well expressed by the Stokes-Einstein equation once the experimental data of viscosity are fitted with the VFT formula.

CRediT authorship contribution statement

Alberto Castellero: Investigation, Writing – original draft, Writing – review & editing, Visualization, Funding acquisition. **Livio Battezzati:** Conceptualization, Writing – original draft, Writing – review & editing, Visualization.

Declaration of Competing Interest

The authors declare that they have no known competing financial interests or personal relationships that could have appeared to influence the work reported in this paper.

Data availability

Data will be made available on request.

Acknowledgments

A. Castellero acknowledges financial support from Università di Torino (Grant "Ricerca locale 2021 Linea A").

References

[1] A.J. Kerns, D.E. Polk, R. Ray, B.C. Giessen, Thermal behavior of Zr-Cu metallic glasses, Mater. Sci. Eng. 38 (1979) 49–53, https://doi.org/10.1016/0025-5416(79)90031-4.
[2] Z. Altounian, T. Guo-hua, J.O. Strom-Olsen, Crystallization characteristics of Cu-Zr metallic glasses from $Cu_{70}Zr_{30}$ to $Cu_{25}Zr_{75}$, J. Appl. Phys. 53 (1982) 4755–4760, https://doi.org/10.1063/1.331304.
[3] E. Kneller, Y. Khan, U. Gorres, The Alloy System Copper-Zirconium, Part II. Crystallization of the glasses from $Cu_{70}Zr_{30}$ to $Cu_{26}Zr_{74}$, Z. Fuer Met 77 (1986) 152–163.
[4] A. Mizuno, T. Harada, M. Watanabe, Effect of minor addition of oxygen on bulk metallic glass formation of binary Cu–Zr alloys via containerless processing, Phys. Status Solidi Basic Res. 257 (2020) 1–5, https://doi.org/10.1002/pssb.202000140.
[5] Y. Wang, J. Yao, Y. Li, Glass formation adjacent to the intermetallic compounds in Cu-Zr binary system, J. Mater. Sci. Technol. 34 (2018) 605–612, https://doi.org/10.1016/j.jmst.2017.09.008.
[6] S. Ganorkar, S. Lee, Y.H. Lee, T. Ishikawa, G.W. Lee, Origin of glass forming ability of Cu-Zr alloys: a link between compositional variation and stability of liquid and glass, Phys. Rev. Mater. 2 (2018), 115606, https://doi.org/10.1103/PhysRevMaterials.2.115606.
[7] S. Ganorkar, Y.H. Lee, S. Lee, Y.Chan Cho, T. Ishikawa, G.W. Lee, Unequal effect of thermodynamics and kinetics on glass forming ability of Cu-Zr alloys, AIP Adv. 10 (2020), 045114, https://doi.org/10.1063/5.0002784.
[8] C.V. Thompson, F. Spaepen, On the approximation of the free energy change on crystallization, Acta Metall. 27 (1979) 1855–1859, https://doi.org/10.1016/0001-6160(79)90076-2.
[9] M. Mohr, R.K. Wunderlich, S. Koch, P.K. Galenko, A.K. Gangopadhyay, K.F. Kelton, J.Z. Jiang, H.J. Fecht, Surface tension and viscosity of $Cu_{50}Zr_{50}$ measured by the oscillating drop technique on board the international space station, Microgravity Sci. Technol. 31 (2019) 177–184, https://doi.org/10.1007/s12217-019-9678-1.
[10] M. Mohr, Y. Dong, D.C. Hofmann, A. Neels, A. Dommann, W.L. Johnson, H. J. Fecht, Thermophysical properties of bulk metallic glasses, H.-J. Fecht, M. Mohr (Eds.). Metallurgy in Space, Springer Nature Switzerland AG, Cham, Switzerland, 2022, pp. 425–450.
[11] Q. Wang, L.M. Wang, M.Z. Ma, S. Binder, T. Volkmann, D.M. Herlach, J.S. Wang, Q.G. Xue, Y.J. Tian, R.P. Liu, Diffusion-controlled crystal growth in deeply undercooled melt on approaching the glass transition, Phys. Rev. B. 83 (2011) 1–5, https://doi.org/10.1103/PhysRevB.83.014202.
[12] Y. Xu, L.P.H. Jeurgens, P. Schützendübe, S. Zhu, Y. Huang, Y. Liu, Z. Wang, Effect of atomic structure on preferential oxidation of alloys: amorphous versus crystalline Cu-Zr, J. Mater. Sci. Technol. 40 (2020) 128–134, https://doi.org/10.1016/j.jmst.2019.10.001.
[13] P.K. Galenko, R. Hanke, P. Paul, S. Koch, M. Rettenmayr, J. Gegner, D.M. Herlach, W. Dreier, E.V. Kharanzhevski, Solidification kinetics of a Cu-Zr alloy: ground-based and microgravity experiments, IOP Conf. Ser. Mater. Sci. Eng. 192 (2017), 012028, https://doi.org/10.1088/1757-899X/192/1/012028.
[14] D.M. Herlach, R. Kobold, S. Klein, Crystal nucleation and growth in undercooled melts of pure Zr, binary Zr-based and ternary Zr-Ni-Cu glass-forming alloys, JOM 70 (2018) 726–732, https://doi.org/10.1007/s11837-018-2782-7.
[15] P. Fopp, M. Kolbe, F. Kargl, R. Kobold, W. Hornfeck, Unexpected behavior of the crystal growth velocity at the hypercooling limit, Phys. Rev. Mater. 4 (2020) 73405, https://doi.org/10.1103/PhysRevMaterials.4.073405.
[16] T.A. Baser, M. Bostrom, M. Stoica, A.R. Yavari, M. Baricco, Analysis of melting and solidification behaviour of glass-forming alloys by synchrotron radiation, Adv. Eng. Mater. 9 (2007) 492–495, https://doi.org/10.1002/adem.200700041.
[17] R.L. Freed, J.B. Vander Sande, A study of the crystallization of two non-crystalline Cu-Zr alloys, J. Non Cryst. Solids 27 (1978) 9–28, https://doi.org/10.1016/0022-3093(78)90032-7.
[18] Z.W. Zhu, H.F. Zhang, W.S. Sun, B.Z. Ding, Z.Q. Hu, Processing of bulk metallic glasses with high strength and large compressive plasticity in $Cu_{50}Zr_{50}$, Scr. Mater. 54 (2006) 1145–1149, https://doi.org/10.1016/j.scriptamat.2005.11.063.
[19] T.A. Baser, J. Das, J. Eckert, M. Baricco, Glass formation and mechanical properties of $(Cu_{50}Zr_{50})_{100-x}Al_x$ (x=0, 4, 5, 7) bulk metallic glasses, J. Alloy. Compd. 483 (2009) 146–149, https://doi.org/10.1016/j.jallcom.2008.07.147.
[20] D. Lee, B. Zhao, E. Perim, H. Zhang, P. Gong, Y. Gao, Y. Liu, C. Toher, S. Curtarolo, J. Schroers, J.J. Vlassak, Crystallization behavior upon heating and cooling in $Cu_{50}Zr_{50}$ metallic glass thin films, Acta Mater. 121 (2016) 68–77, https://doi.org/10.1016/j.actamat.2016.08.076.

[21] A.T. Dinsdale, SGTE data for pure elements, Calphad 15 (1991) 317–425, https://doi.org/10.1016/0364-5916(91)90030-N.
[22] K. Russew, L. Stojanova, S. Yankova, E. Fazakas, L.K. Varga, Thermal behavior and melt fragility number of $Cu_{100-x}Zr_x$ glassy alloys in terms of crystallization and viscous flow, J. Phys. Conf. Ser. 144 (2009) 2–6, https://doi.org/10.1088/1742-6596/144/1/012094.
[23] N.A. Mauro, M. Blodgett, M.L. Johnson, A.J. Vogt, K.F. Kelton, A structural signature of liquid fragility, Nat. Commun. 5 (2014) 4616, https://doi.org/10.1038/ncomms5616.
[24] H. Zhang, C. Zhong, J.F. Douglas, X. Wang, Q. Cao, D. Zhang, J.-Z. Jiang, Role of string-like collective atomic motion on diffusion and structural relaxation in glass forming Cu-Zr alloys, J. Chem. Phys. 142 (2015), 164506, https://doi.org/10.1063/1.4918807.
[25] A.E. Lagogianni, J. Krausser, Z. Evenson, K. Samwer, A. Zaccone, Unifying interatomic potential, g(r), elasticity, viscosity, and fragility of metallic glasses: analytical model, simulations, and experiments, J. Stat. Mech. Theory Exp. 2016 (2016), 084001, https://doi.org/10.1088/1742-5468/2016/08/084001.
[26] D.V. Louzguine-Luzgin, G. Xie, W. Zhang, A. Inoue, Influence of Al and Ag on the devitrification behavior of a Cu-Zr glassy alloy, Mater. Trans. 48 (2007) 2128–2132, https://doi.org/10.2320/matertrans.MF200633.
[27] S. Pauly, J. Das, N. Mattern, D.H. Kim, J. Eckert, Phase formation and thermal stability in Cu-Zr-Ti(Al) metallic glasses, Intermetallics 17 (2009) 453–462, https://doi.org/10.1016/j.intermet.2008.12.003.
[28] D.R. Macfarlane, Continuous cooling (CT) diagrams and critical cooling rates: a direct method of calculation using the concept of additivity, J. Non Cryst. Solids 53 (1982) 61–72, https://doi.org/10.1016/0022-3093(82)90018-7.
[29] W.H. Wang, J.J. Lewandowski, A.L. Greer, Understanding the glass-forming ability of $Cu_{50}Zr_{50}$ alloys in terms of a metastable eutectic, J. Mater. Res. 20 (2005) 2307–2313, https://doi.org/10.1557/JMR.2005.0302.
[30] T. Cullinan, I. Kalay, Y.E. Kalay, M. Kramer, R. Napolitano, Kinetics and mechanisms of isothermal devitrification in amorphous $Cu_{50}Zr_{50}$, Metall. Mater. Trans. A 46 (2015) 600–613, https://doi.org/10.1007/s11661-014-2661-y.
[31] S.T. Zhang, Q. Wang, T.T. Liu, J.J. Liu, Controlling crystallization process and thermal stability of a binary Cu-Zr bulk metallic glass via minor element addition, Int. J. Mod. Phys. B 29 (2015), 1550178, https://doi.org/10.1142/S0217979215501787.
[32] K. Kelton, L. Greer, Nucleation in Condensed Matter: Applications in Materials and Biology, Pergamon Materials Series, Elservier, Amsterdam, The Netherlands, 2010.
[33] N. Iwamoto, H. Yokoo, Joining of zirconia to metals using Zr-Cu alloy, Eng. Fract. Mech. 40 (1991) 931–940, https://doi.org/10.1016/0013-7944(91)90254-X.
[34] L. Battezzati, A.L. Greer, The viscosity of liquid metals and alloys, Acta Metall. 37 (1989) 1791–1802, https://doi.org/10.1016/0001-6160(89)90064-3.
[35] A.K.A. Lu, D.V. Louzguine-Luzgin, Crystal nucleation and growth processes in Cu-rich glass-forming Cu-Zr alloys, J. Chem. Phys. (2022) 157, https://doi.org/10.1063/5.0097023.
[36] H.-M. Hsiao, S.M. Liang, R. Schmid-Fetzer, Y.-W. Yen, Thermodynamic assessment of the Ag-Zr and Cu-Zr binary systems, Calphad 55 (2016) 77–87, https://doi.org/10.1016/j.calphad.2016.08.001.
[37] L. Battezzati, A. Castellero, Nucleation and the properties of undercooled melts, Trans Tech Publications Ltd., Uetikon-Zurich, Switzerland, 2002, pp. 1–80. M. Magini, F. Wohlbier (Eds.), Mater. Sci. Found.
[38] S.V. Ketov, Y.P. Ivanov, B. Putz, Z. Zhang, J. Eckert, A.L. Greer, Atomic diffusivities in amorphous and liquid Cu-Zr: kirkendall effects and dependence on packing density, Acta Mater. 214 (2021), 116993, https://doi.org/10.1016/j.actamat.2021.116993.